# Hydrodynamic Characteristics of New Floating Wind-Wave Energy Combined Power Generation Devices Under Typhoon-Wave-Current Coupling

*ZHAO Yongfa, KE Shitang*, YUN Yiwen*

Department of Airport and Civil Engineering, Nanjing University of Aeronautics and Astronautics, Nanjing 211106, P. R. China

(Received 10 April 2022; revised 27 May 2022; accepted 20 July 2022)

**Abstract:** The South China Sea is rich in wind and wave energy resources, and the wind-wave combined power generation device is currently in the concept research and development stage. In recent years, extreme sea conditions such as super typhoons have frequently occurred, which poses a serious challenge to the safety of offshore floating platforms. In view of the lack of safety analysis of wind-wave combined power generation devices in extreme sea conditions at present, this paper takes the OC4-WEC combined with semi-submersible wind turbine (Semi-OC4) and the oscillating buoy wave energy converter as the research object, and establishes a mesoscale WRF-SWAN-FVCOM (W-S-F) real-time coupling platform based on the model coupling Toolkit (MCT) to analyze the spatial and temporal evolution of wind-wave-current in offshore wind farms during the whole process of super typhoon "Rammasun" transit. Combined with the medium/small scale nested method, the flow field characteristics of OC4-WEC platform are analyzed. The results show that the simulation accuracy of the established W-S-F platform for typhoon track is 42.51% higher than that of the single WRF model. Under the action of typhoon-wave-current, the heave motion amplitude of OC4-WEC platform is reduced by 38.1%, the surge motion amplitude is reduced by 26.7%, and the pitch motion amplitude is reduced by 23.4%.

**Key words:** extreme sea conditions; wind and wave combined power generation; wave nonlinearity

**CLC number:** TN925 **Document code:** A **Article ID:** 1005-1120(2022)S-0082-08

## 0 Introduction

The South China Sea is rich in wind and wave energy resources. Wind and wave combined power generation has more advantages in economic cost than simple wind power generation[1]. However, in recent years, extreme sea conditions such as ultra-strong typhoons have frequently occurred. The emergence of gales and waves poses a serious threat to the safety of offshore platforms. The wind-wave combined power generation device in China is still in the conceptual development stage. The existing specifications do not involve the hydrodynamic load safety design of such complex integrated devices. Therefore, it is of great significance to study the hydrodynamic load characteristics of wind-wave combined power generation devices under typhoon-wave-current extreme conditions.

In the view of structural design of wind-wave combined power generation devices, scholars have proposed different design schemes[2-5]. Bachynski et al.[6] proposed a 5 MW wind turbine and three point suction wave energy converter (WEC) combined system based on the tension leg platform (TLP). Based on the foundation WindFloat of the semi-submersible wind turbine platform, a floating structure of wind turbine with very large support is integrated with three different types of WEC, namely the oscillating water column, the spherical wave energy device and the oscillating float WEC. Hu et al.[7] stud-

*Corresponding author, E-mail address: keshitang@163.com.

**How to cite this article**: ZHAO Yongfa, KE Shitang, YUN Yiwen. Hydrodynamic characteristics of new floating wind-wave energy combined power generation devices under typhoon-wave-current coupling[J]. Transactions of Nanjing University of Aeronautics and Astronautics, 2022, 39(S): 82-89.

http://dx.doi.org/10.16356/j.1005-1120.2022.S.011

ied the power generation of the wind-wave combined power generation device combining the WindFloat platform and the oscillating float without considering the platform motion. The above studies show that compared with the independent floating offshore wind turbine, the addition of WEC can increase the total power output. Among them, the oscillating float WEC has the advantages of high conversion efficiency, low cost and stable output power, which is suitable for the areas with high wave energy density in the South China Sea. Liu et al.[8] compared the hydrodynamic performance of OC4, WindFloat, Ideol three kinds of semi-submersible wind turbine foundation, and found that OC4 foundation with large drainage volume and deep water has better comprehensive performance. Therefore, this paper selects the oscillating float WEC and the OC4 floating wind turbine platform as the object of combination.

There is a strong coupling between typhoons, ocean waves and ocean currents, and the traditional single flow field simulation method cannot accurately capture the feedback information of waves and ocean currents during typhoons. In this paper, the semi-submersible wind turbine (Semi-OC4) and oscillating buoy wave energy device (WEC) combined wind-wave combined power generation device (OC4-WEC) are taken as the research object. Based on the model coupling toolkit (MCT), a mesoscale WRF-SWAN-FVCOM (W-S-F) real-time coupling platform is established to analyze the spatial and temporal evolution of wind-wave-currents in an offshore wind farm during the whole process of super typhoon "Rammasun" transit. Combined with the medium/small scale nested method, the flow field characteristics of OC4-WEC platform are analyzed.

## 1 Project Profile

In this paper, the OC4 semi-submersible wind turbine platform is selected as a case study, and the hemispherical bottom cylindrical WEC which is better adapted to the change of flow fields during heaves is combined with it. The combination form of the OC4 semi-submersible turbine platform and the hemispherical bottom cylindrical WEC is shown in Fig.1. The wind turbine legs are fixedly connected by trusses. The wind turbine tower is mounted on the middle column of the semi-submersible platform. WEC is installed on the platform side between the trusses and generates electricity along the direction of the fixed rod through its relative heave motion with the platform. The basic scale parameters of the platform are shown in Table 1.

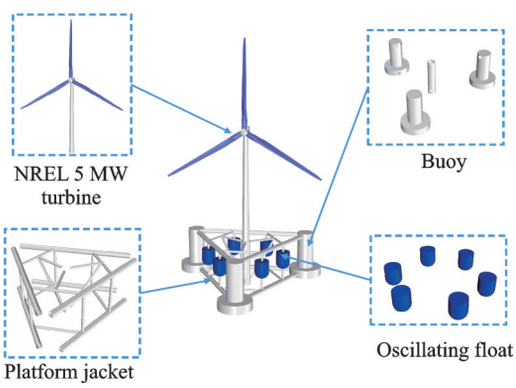


Fig.1 Combination form of the OC4 semi-submersible turbine platform and the hemispherical bottom cylindrical WEC

**Table 1 Basic main scale parameters of platform** m

| Design parameter | Numerical value |
|---|---|
| Center distance of upper column | 189 |
| Depth from platform bottom to water surface | 85 |
| Diameter of central column | 101.0 |
| Diameter of upper column | 67.0 |
| Diameter of foundation column | 32.5 |
| Oscillating float diameter | 123.2 |
| Eating depth of float | 29.0 |
| Water depth of platform center of gravity | 148.0 |

## 2 Mesoscale Wind-Wave-Current Coupling Field Simulation

### 2.1 Mesoscale W-S-F coupling platform

Fig.2 shows the data transfer diagram of W-S-F coupling platform. The platform calls each submode for data exchange through MCT. Among them, weather research and forecast (WRF) transmits wind speed to simulating waves nearshore

(SWAN) and FVCOM to generate the driving wind field of wave-current motion. FVCOM transmits sea surface temperature to WRF, affecting the typhoon intensity and path. FVCOM transmits current tidal level and velocity to SWAN, affecting the change of wave waveform elements. SWAN transmits waveform elements to FVCOM, affecting the movement process and distribution form of currents. SWAN transmits waveform elements to WRF, affecting the wind profile and motion process of typhoon[9-10].

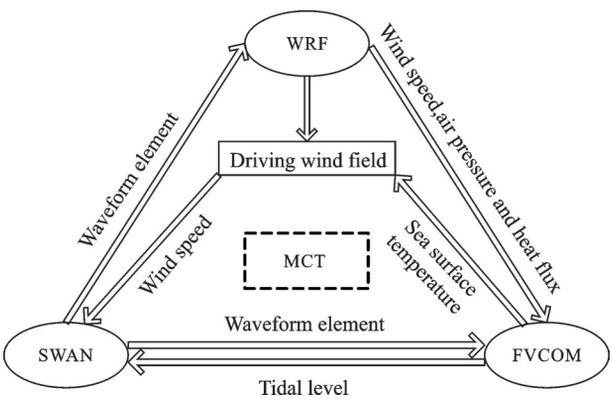


Fig.2 Schematic diagram of data transfer of W-S-F coupling platform

## 2.2 Result analysis of W-S-F platform

This paper simulates Typhoon 9 "Rammasun" in 2014. Its maximum wind level reached 17, the strongest typhoon since the founding of China. Fig. 3 shows the history curves of the typhoon, waves and currents in the wind farm. It can be seen that the basic wind speed at 10 m on the sea surface shows M-shaped variation with different stages of typhoon transit, and the maximum basic wind speed is 42.7 m/s, which appears in the eye wall area after the typhoon (55 h). Waves and currents have a certain lag inertia with the response of the typhoon field, and the maximum wave height is 7.22 m. The maximum current velocity is 2.13 m/s.

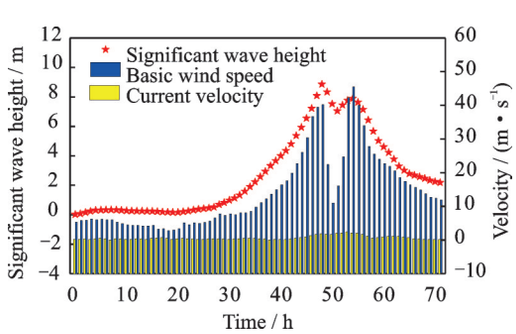


Fig.3 Time-history curves of typhoon, waves and currents

Fig.4 shows the schematic diagram of typhoon-wave-current coupling simulation results when the typhoon eyewall passes through a wind farm in South China Sea. It can be seen that during the typhoon, the wind field revolves counterclockwise around the typhoon eye, and the wind speed in the

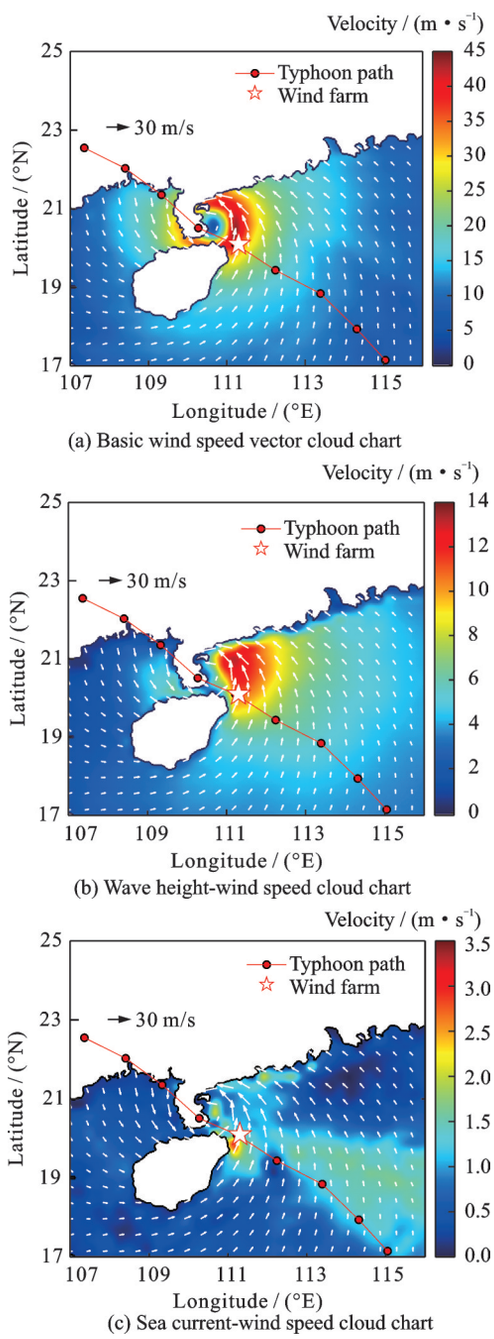


Fig.4 Diagram of simulation results of typhoon-wave-current coupling

rear eye wall is greater than that in the front eye wall. The spatial distribution of the wave height shows a "crescent" shape. A small wave area is formed near the typhoon eye and a large wave area is formed on the right side. The response of the current field to the wind field has significant hysteresis and right deviation. The current flows counterclockwise around the rear of the typhoon eye. The flow velocity on the right side is significantly greater than that on the left side, and there is a recirculation zone with a large flow velocity behind the right of the typhoon eye. When the typhone landed Hainan and Guangdong, the wave height decreased rapidly and the current velocity increased significantly due to the nearshore shallow water effect.

## 3 Small Scale CFD Simulation

### 3.1 Operation setting

In order to ensure the stability of the structure, the wind-wave combined power generation device is in shutdown state under extreme sea conditions, and the wind wheel and oscillating floater are fixed with the platform. The inflow boundary of CFD simulation is selected from the typhoon-wave-current parameters with the maximum wind speed of wind farm simulated by the W-S-F coupling platform during the typhoon transit. The specific working condition settings are shown in Table 2.

**Table 2 Condition settings**

| Parameter | Numerical value |
|---|---|
| Significant wave height/m | 7.22 |
| Period/s | 9.14 |
| Wave length/m | 98.77 |
| Basic wind speed/(m•s$^{-1}$) | 42.7 |
| Wind profile index | 0.102 1 |
| Current velocity/(m•s$^{-1}$) | 2.13 |
| Water depth/m | 80 |
| Wind wheel status/(°) | 0 |
| Oscillating float state | Fixation |

### 3.2 CFD simulation method and parameter settings

In the construction of the numerical calculation area of waves, the Eulerian two-phase flow model, the Eulerian model, is adopted. The seawater is taken as the heavy fluid, and the main phase is set. The air is the light fluid, and the secondary phase is set. This model considers the viscosity of the fluid, and its basic control equation is composed of the continuity equation and the momentum conservation equation. The Reynolds-averaged Navier-Stokes (RANS) method is used to describe the turbulent motion of the fluid, and the volume of fluid (VOF) model is used to simulate and track the motion changes of the gas-liquid two-phase interface, and the free surface of the wave. The most widely used $k$-$\varepsilon$ turbulence model is selected, and the turbulent kinetic energy and dissipation term are in the second-order format.

The continuity equation is a fluid mechanics expression of the principle of mass conservation. For the unsteady flow of compressible fluid, the continuity equation is

$$\frac{\partial \rho}{\partial t}+\nabla\cdot(\rho V)=0 \tag{1}$$

where $\rho$ represents the fluid density, $t$ the time, and $V$ the velocity.

The momentum conservation equation includes the N-S equation that completely describes the fluid motion and the Euler equation that describes the motion of inviscid fluid. The vector form of the N-S equation is expressed as

$$F-\frac{1}{\rho}\nabla P+\upsilon\nabla^2 V=\frac{\partial V}{\partial t}+(V\cdot\nabla)V \tag{2}$$

where $F$ represents the volume force and the kinematic viscosity coefficient.

Fig. 5 shows the grid division diagram of typhoon- wave-current numerical pool. The grid division adopts the mixed grid discrete form, and the whole calculation domain is divided into internal and external parts. The core encryption area adopts tetrahedral unstructured grid. The height of the first layer of the wind turbine structure wall is 0.002 m, the gradient rate is 1.1, and the $y+$ value is less than 30. The outer region is more regular, using hexahedral structured grid with resolution of $\Delta x=L/150$, $\Delta y=H/6$, $\Delta z=H/10$.

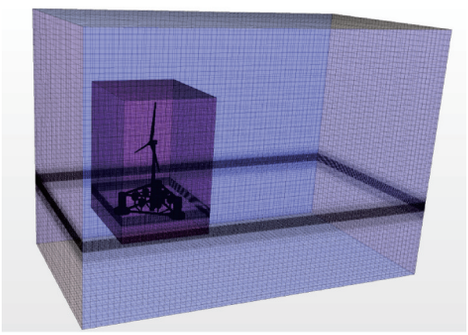

(a) Overall grid division

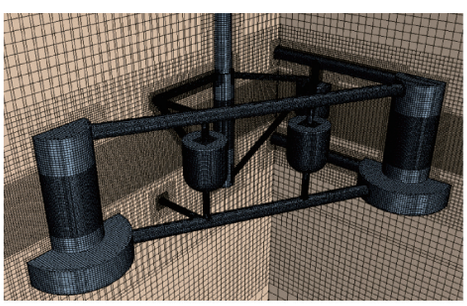

(b) Platform grid division

Fig.5 Diagram of numerical pool grid division

### 3.3 Movement characteristics analysis

Under extreme conditions, in order to ensure the structural safety, the wind wheel and oscillating float of the wind-wave combined power generation device are in a fixed state. At this time, the wind turbine blade is not rotating and is in a propulsive state. The thrust of the wind wheel is small, and the wave force plays a major role in the motion of the floating platform. In order to study the influence of the float of the wind-wave combined power generation platform on the motion of the semi-submersible platform, this paper compares the motion characteristics of the wind-wave combined power generation platform and the semi-submersible platform under the condition of typhoon and wave. Fig. 6 shows the free attenuation curves of the heave motion of the two platforms. It can be seen that the installation of the oscillating float significantly increases the inherent period of the heave motion of the semi-submersible platform, indicating that the installation of the oscillating float increased the viscous damping of the semi-submersible platform.

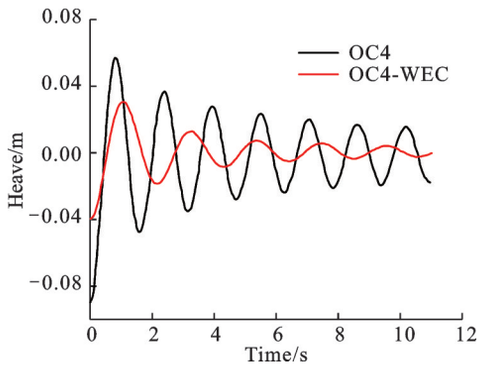


Fig.6 Free attenuation curves in heave direction of the two platforms

### 3.4 Flow field analysis

Fig. 7 shows a schematic diagram of the free surface change during the wave climbing process of OC4-WEC platform in a wave period. The jacket and wind turbine are hidden, and only the buoy and float are shown. The wave propagates from the left to the right. It can be seen that the wind ripple appears on the windward surface of the wave, and the phenomenon of wind driven wave is obvious. Therefore, the effect of load on OC4-WEC platform is different from that on pure wave field or pure water field. In Fig.7(a), after the wave encounters buoy 1 in the propagation process, the pitch motion of OC4-WEC platform intensifies under the action of wave uplift. Due to the viscous water body and the obstruction of the cylinder, some waves will climb up along the buoy against the wave. At the same time, the other part of the water will be divided into two streams of impact flow, which propagates forward along both sides of buoy 1, and the refluent flow can be observed at buoy 2 and buoy 5. In Fig.7 (b), when the wave crest passes through buoy 1, the water flow on both sides finally causes strong nonlinear superposition on the back of buoy 1 column, and makes the amplification rate of the wave surface increase rapidly, forming the "cocktail" effect. The wave climbs along the buoy 1 and overtook. In Fig.7(c), when the wave crest passes through float 2, the water separation occurs at float 2, and the water body at the back of float 1 begins to fall. Due to the influence of floats and columns on wave shielding, wave energy is continuously dissipated, and the climbing of waves in float 3 and float

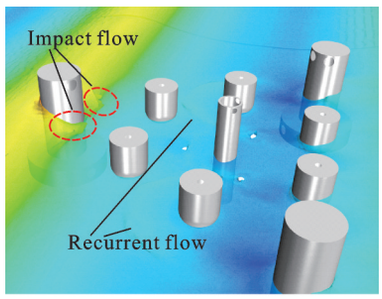


(a) Wave crest through buoy 1

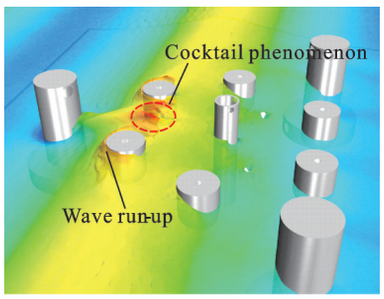


(b) Wave crest through float 1

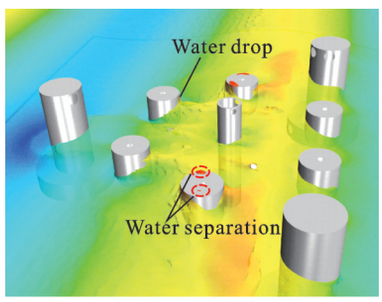


(c) Wave crest through float 2

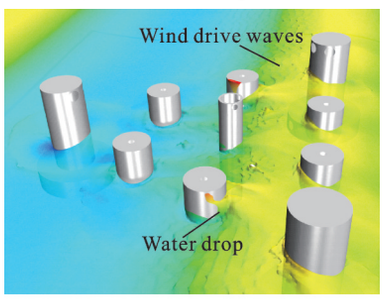


(d) Wave crest through buoy 2

Fig.7 Diagram of free surface change during wave climbing

4 is gradually reduced.

### 3.5 Hydrodynamic load analysis

Based on the symmetry of OC4-WEC platform, Fig.8 shows the wave force of three floats with different relative positions of OC4-WEC platform. It can be seen that the maximum longitudinal wave force on the float is 1.21e6, and the maximum transverse wave force is −1.76e5. The longitudinal wave load is the dominant load. The buoy is subjected to wave forces in different directions in different wave phases. In the period from wave trough ($3T/4$) to wave crest ($T/4$), the front of the buoy is subjected to positive pressure under the attack of waves, and in the period from wave crest ($T/4$) to wave trough ($3T/4$), the back of the buoy is subjected to positive pressure. It can be seen in Fig.8 (a) that there are obvious secondary wave peaks in float 1 and float 2. As the water slowly falls back along the back of the float, it moves along the side of the float in the opposite direction to the incident wave, and superimposes with the incident wave to form a secondary impact. In practice, it should be avoided that the frequency corresponding to the secondary wave peak is close to the natural frequency of the wind turbine so as to avoid resonance and damage of the wind turbine. Because of the wave shielding effect of the OC4-WEC platform, the wave energy inside the platform is continuously dissipated, the wave force acting on float 3 is small, and no obvious secondary wave peak is observed. It can be seen from Fig.8(b) that the lateral wave force of the float is much smaller than that of the forward wave force, but it has stronger nonlinear characteristics. From the above analysis, it can be con-

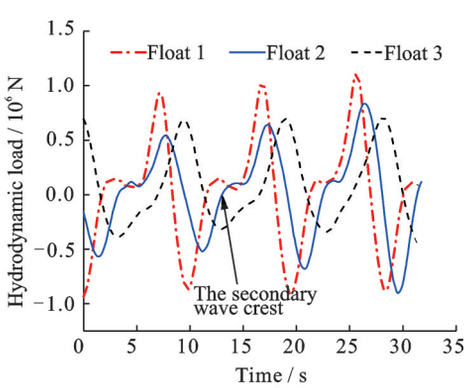


(a) Directional wave force

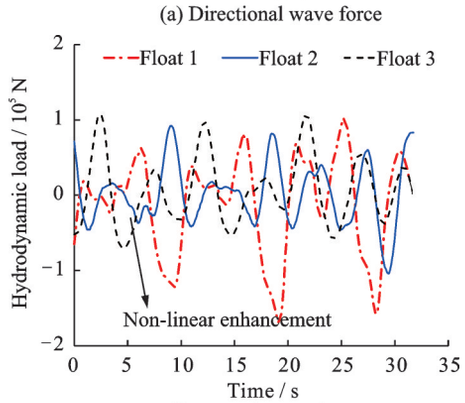


(b) Lateral wave force

Fig.8 Wave force time curves of OC4-WEC float

cluded that the existence of the buoy, the float and the jacket inside the platform has a strong nonlinear effect on the wave inside the platform, which is mainly reflected in the lateral wave force.

## 4 Conclusions

Based on the established W-S-F real-time coupling simulation platform, the parameters of typhoon, waves and currents of an offshore wind farm during the transit of typhoon "Rammasun" are refined, and the hydrodynamic load characteristics of OC4-WEC under extreme conditions of typhoon, waves and currents are simulated and analyzed by using the downscaling method of middle/small scale nested. It is proposed that the additional wave influence coefficient is used as an indicator to comprehensively evaluate the influence of the layout of the platform structure on the wave load of its internal structure. The main conclusions are as follows:

(1) The established W-S-F real-time coupling simulation platform can accurately simulate the spatio-temporal distribution and evolution characteristics of typhoon, wave and current in the whole process of typhoon transit. The simulation accuracy of typhoon path is 42.51% higher than that of single WRF model.

(2) Compared with the semi-submersible (Semi-OC4) platform, the amplitude of OC4-WEC platform decreases in the motions of surges, heaves and pitches, which are greatly affected by the frontal waves. The amplitude of heave motions decreases by 38.1%, the amplitude of surge motions decreases by 26.7%, and the amplitude of pitch motion decreases by 23.4%, indicating that the existence of oscillating buoy increases the dissipation of wave energy on the platform and improves the stability of the platform.

(3) There are obvious secondary wave peaks in buoy 1 and buoy 2 of the OC4-WEC platform. The OC4-WEC platform has the wave shielding effect, and the wave energy inside the platform is continuously dissipated. The wave force acting on buoy 3 is small, and no obvious secondary wave peak phenomenon is observed.

**References**

[1] DENG C W, LI C Y. Development of the islands and reefs in the south china sea: Wind power and wave power generation[J]. Periodical of Ocean University of China, 2015, 45(9): 7-14.

[2] CHEN W, GAO F, MENG X, et al. W2P: A high-power integrated generation unit for offshore wind power and ocean wave energy[J]. Ocean Engineering, 2016, 128: 41-47.

[3] MICHAILIDES C, GAO Z, MOAN T. Experimental and numerical study of the response of the offshore combined wind/wave energy concept SFC in extreme environmental conditions[J]. Marine Structures, 2016, 50: 35-54.

[4] YANG Y, MUSA B, JIN W. Wind-wave coupling effects on the fatigue damage of tendons for a 10 MW multi-body floating wind turbine[J]. Ocean Engineering, 2020, 217: 107909.

[5] MINNAN Y, QINGSONG L, CHUN L. Effects of heave plate on dynamic response of floating wind turbine Spar platform under the coupling effect of wind and wave[J]. Ocean Engineering, 2020, 201: 107103.

[6] BACHYNSKI E E, MOAN T. Point absorber design for a combined wind and wave energy converter on a tension-leg support structure[C]//Proceedings of International Conference on Offshore Mechanics and Arctic Engineering. Nantes, France: American Society of Mechanical Engineers, 2013: 55423.

[7] HU J, ZHOU B, VOGEL C, et al. Optimal design and performance analysis of a hybrid system combing a floating wind platform and wave energy converters[J]. Applied energy, 2020, 269: 114998.

[8] LIU Z, FAN T, CHEN C, et al. Comparison on hydrodynamic performance of three kinds of typical semi-submersible floating foundations of offshore wind turbine[J]. China Offshore Platform, 2021, 36(2): 1-10.

[9] PORTALAKIS P, TOMBROU M, KALOGIROS J. Investigation of air-sea turbulent momentum flux over the aegean sea with a wind-wave coupling model[J]. Atmosphere, 2021, 12(9): 1208.

[10] YUN Y W, KE S T, WANG S, et al. Effects of ocean movement on the horizontal wind speed characteristics throughout a typhoon landing process[J]. Acta Aerodynamica Sinica, 2021, 39(4): 153-161.

**Acknowledgements** This work was jointly funded by the National Key Research and Development Projects (No. 2017YFE0132000), the National Natural Science Foundation of China (Nos. 5211101879, 52078251, 52108456),

and the Natural Science Foundation of Jiangsu Province (Nos. BK20211518, BK20210309).

**Authors** Mr. **ZHAO Yongfa** is a graduate student at Nanjing University of Aeronautics and Astronautics. His research is focused on wind and wave combined power generation.

Prof. **KE Shitang** received the Ph.D. degree in civil engineering from Tongji University in 2012. He is a professor at Nanjing University of Aeronautics and Astronautics. His research has focused on wind and wave combined power generation

**Author contributions** Mr. **ZHAO Yongfa** investigated the conceptualization, methodology and software of the study, and wrote the draft. Prof. **KE Shitang** contributed to the conceptualization, wrote the literature review, and supervised the research. Mr. **YUN Yiwen** contributed to the conceptualization and literature review. All authors commented on the manuscript draft and approved the submission.

**Competing interests** The authors declare no competing interests.

(Production Editor: ZHANG Bei)

# 台风-浪-流耦合作用下新型浮式风能-波浪能联合发电装置水动力特性

赵永发，柯世堂，员亦雯

（南京航空航天大学土木与机场工程系，南京 211106，中国）

**摘要**：中国南海风能-波浪能资源丰富，风浪联合发电装置目前却处于概念研发阶段，加上近几年超强台风等极具破坏力的极端海况频繁出现，对海上浮式平台安全性提出了严峻挑战。针对现阶段研究缺少对风浪联合发电装置在极端海况的安全性分析，本文以半潜式风力机（Semi-OC4）与振荡浮子式波浪能装置相结合的风浪联合发电装置（OC4-WEC）为研究对象，基于MCT（Model coupling toolkit）建立中尺度WRF-SWAN-FVCOM（W-F-S）实时耦合平台，分析超强台风“威马逊”过境全过程海上风电场风-浪-流的时空演变；再结合了中/小尺度嵌套的方法分析了OC4-WEC平台的流场特性。结果表明：建立的W-S-F平台对台风路径的模拟精度较单WRF模式提高了42.51%；台风-浪-流作用下OC4-WEC平台较半潜式风力机垂荡运动幅值减小38.1%，纵荡运动幅值减小26.7%，纵摇运动幅值减小23.4%

**关键词**：极端海况；风浪联合发电；波浪非线性